17th World Conference on Nondestructive Testing, 25-28 Oct 2008, Shanghai, China

Fiber Bragg Gratings and Two Wave Mixing Spectral Demodulator System for Impact Detection and Localization

Goutham KIRIKERA, Oluwoseyi BALOGUN, Sridhar KRISHNASWAMY
Center for Quality Engineering and Failure Prevention,
Northwestern University, Evanston, IL 60208, USA.

ABSTRACT

Multiplexed fiber Bragg grating (FBG) sensors capable of dynamically measuring high frequency (>200KHz) ultrasonic waves using a two wave mixing spectral demodulator has been reported by us previously. The two-wave mixing spectral demodulator enables multiplexing of several FBG sensors and also acts as a high pass filter eliminating low frequency thermal drift and vibrational noise without the need for stabilization as required by other interferometric demodulation schemes. We have demonstrated that this system is capable of monitoring and locating of impact events if several FBG sensors are used. In this paper, we present recent results that have extended our original architecture to take into account the directional dependence of FBG sensor sensitivity to propagating ultrasonic waves. Since the FBG is highly directionally dependent at high frequencies, a simple rosette FBG pattern is implemented enabling effective detection of impact from any location.

Keywords: structural health monitoring, fiber sensors

1. INTRODUCTION

Fiber Bragg grating (FBG) sensors have been developed for a variety of applications including optical remote sensing of strain, temperature, and pressure. These sensors offer special advantages: they are light-weight, resistant to corrosion, immune to electromagnetic interference, and can be multiplexed thus allowing for the simultaneous measurement of strain, temperature and pressure at multiple locations. Several applications of FBG sensors in health monitoring of structures have been reported in the literature[1-8].

In this paper, we describe a recently-developed two-wave mixing spectral demodulator[9-11] that is used in conjunction with a network of FBG sensors to monitor high frequency dynamic strains (>10KHz). Unlike existing demodulation methods, the TWM demodulator enables monitoring high-frequency dynamic strains simultaneously from several FBG sensors. Moreover, the system is immune to quasistatic drift caused by temperature or quasistatic strains. As such the system is ideally suited for monitoring stress waves caused by impact or acoustic emissions.

In the following sections, the principle of a high-power TWM spectral demodulation is briefly described, followed by a description of the system performance in terms of frequency response etc. An application to impact monitoring is then described. Finally, preliminary results from a low-power TWM spectral demodulator with significantly lower system cost is described.

2 HIGH-POWER TWO-WAVE MIXING SPECTRAL DEMODULATOR:

The system diagram for a TWM interferometer used as a wavelength demodulator for the FBG sensor is shown in Figure 1. The FBG sensor is illuminated by a broadband amplified spontaneous emission (ASE) source in the C-band, and the reflected light is coupled by a circulator into an Erbium doped fiber amplifier (EDFA) with output power 500mW (hence called high-power system). The amplified light is split into pump and signal beams that travel unbalanced optical paths to the PRC. The light reflected from the FBG sensor will undergo *spectral* shift due to strain-induced changes in the Bragg-reflectivity. The sensors by themselves are sensitive to both quasi-static and dynamic strains, and are also subject to thermal drift.

However, since the TWM demodulator is adaptive, the system will only track dynamic strains, and will automatically compensate for quasistatic drifts.

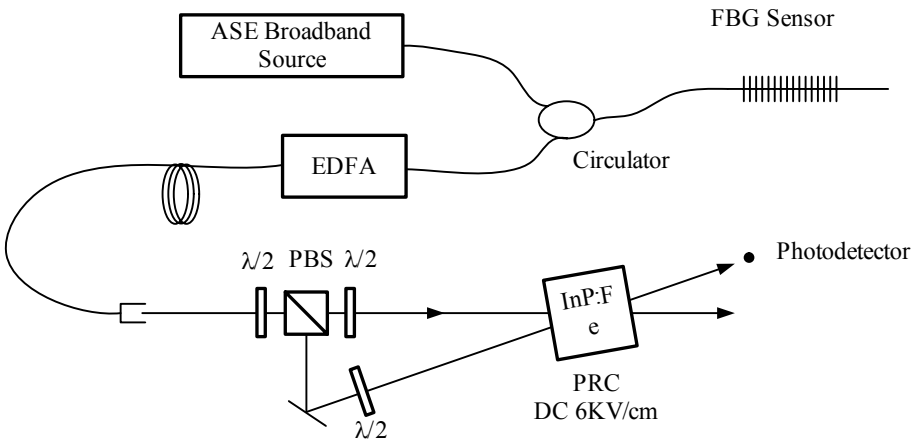

Figure.1 System diagram of TWM fiber Bragg-grating sensor demodulator.

For TWM to work as a wavelength demodulator of dynamic FBG spectral shifts, the basic idea is similar to that of the Mach-Zehnder Interferometer (MZI) or other path unbalanced interferometric demodulation schemes. In these schemes, the wavelength shift is tracked as a phase-shift that results from the same input beam traveling two different optical path lengths. The main point is that the signal and pump beams in the TWM are both obtained from the same FBG sensor and therefore are both subject to the same wavelength shift. However, the two beams are made to travel unbalanced paths prior to mixing in the PRC. Therefore the spectral shift is effectively converted to an optical phase difference which is given by:

$$\varphi(t) = -\frac{2\pi d}{\lambda^2}\Delta\lambda(t), \qquad (1)$$

where d is the optical path difference (OPD), λ is the nominal center wavelength of the light from the Bragg-grating sensor; Δλ is the time-varying shift in the wavelength caused by the measurand.

In order to demonstrate wavelength demodulation, we applied a 10 kHz, 10 με strain onto the FBG sensor and measured the wavelength demodulated signal amplitude at different values of the optical path difference. As shown in Figure 2, an intermittent DC field is applied from 1ms to 6ms with respect to a reference trigger, and the photorefractive grating initially builds up. The dynamic strain is applied as a toneburst starting from 2ms to 6ms.When the OPD equals to zero, although the TWM energy gain[12] is at its maximum, there is no detected wavelength demodulated signal because there is no OPD to convert the wavelength shift into phase shift. As the OPD increases, the wavelength demodulated signal starts to appear. The signal reaches maximum when OPD equals 8mm and beyond that further increasing of the OPD causes the signal to drop.

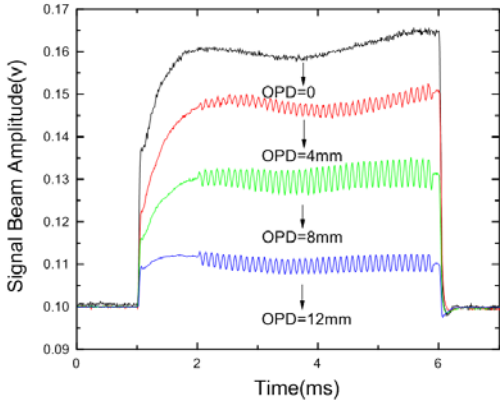

Figure 2 Wavelength demodulated signal at different values of OPD. An intermittent DC field is applied to the PRC starting from 1ms to 6ms and a 10 kHz 10 με strain is applied to the FBG from 2ms to 6ms

2.1 Adaptivity to low-frequency drift:

One of the advantages of using the two-wave mixing interferometer as a wavelength demodulator is its adaptivity to low frequency drift. As mentioned earlier, the two-wave mixing interferometer is automatically adaptive to low frequency strain or temperature drift of the FBG sensor. In order to show adaptivity to quasistatic strain, we applied a frequency sweep signal from 10Hz to 1.2 kHz with a constant magnitude of 10με. Figure 3 shows the response of the wavelength demodulator to this frequency sweep signal. The demodulator ignores the low frequency strain applied in the beginning and starts to respond to frequencies above 600Hz.

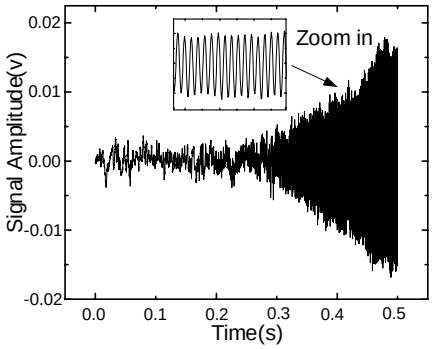

Figure 3 TWM wavelength demodulator response to a frequency sweep signal from 10 Hz to 1.2 kHz.

Figure 4 demonstrates the adaptivity to quasistatic strain more clearly in the frequency domain. Figure 4 (a) is the Fourier spectrum of the applied sweep signal, Figure 4 (b) is the spectrum of the system response to the sweep signal, and Figure 4 (c) is the system transfer function (modulus) calculated by dividing the system response spectrum by the sweep signal spectrum. From Figure 4, it is clear that the TWM wavelength demodulator is adaptive to low frequency strains and acts like a high pass filter with a cut-off frequency of 600 Hz. The cut-off frequency of the system is directly related to the response time of the InP:Fe PRC.

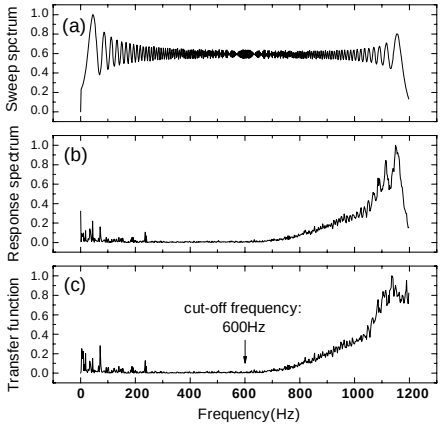

Figure 4 (a) Fourier spectrum of the applied frequency sweep signal from 10 Hz to 1.2 kHz. (b) Fourier spectrum of the response of the TWM wavelength demodulator. (c) Transfer function of the TWM wavelength demodulator. The cut-off frequency is seen to be around 600 Hz for this configuration

2.2 Multiplexing of FBG sensors:

In addition to adaptivity to low frequency drift, another major advantage of using TWM as wavelength demodulator for FBG sensors is that it can be multiplexed without significant increase in cost. This is because all the channels (wavelengths) share the same PRC and there is no expensive feedback electronics involved.

We now demonstrate a four-channel TWM wavelength demodulator together with quasi-static drifts monitoring. The experimental configuration is shown in Figure 5. Four 0.15nm line-width FBG sensors are connected in series and are centered at 1536nm, 1540nm, 1544nm and 1548nm respectively. The experimental configuration is similar to that of the single channel configuration shown in Figure 1 except that after the PRC, there is a free space to fiber coupler to couple the free space light into a set of four band drop filters, and also there is an optical spectrum analyzer monitoring the transmitted light through the FBG sensors.

In order to show that four FBG sensors can be monitored simultaneously, we applied 10 kHz 5 με strain on FBG sensor 1 (1536nm), 5 kHz 5 με on FBG sensor 2 (1540nm), 2 kHz 5 με on FBG sensor 3 (1544nm) and 20 kHz 5 με on FBG sensor 4 (1548nm) simultaneously. Figure 6 shows that the dynamic strain from four channels can be demodulated simultaneously.

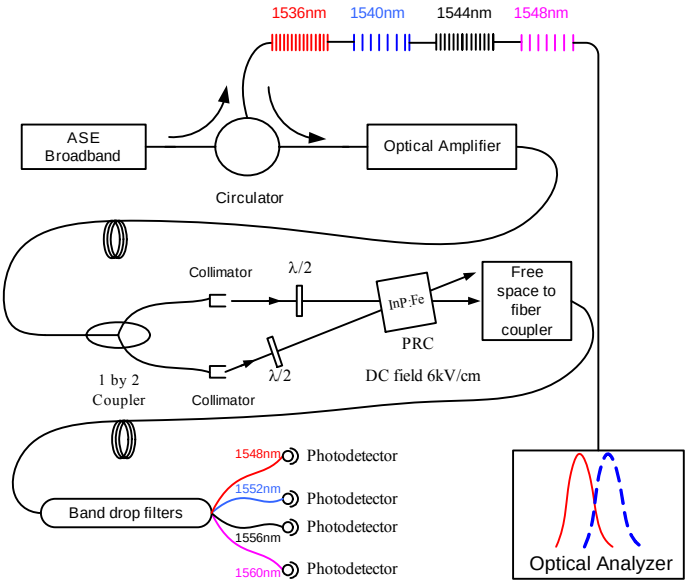

Figure 5 Experimental configuration for the four-channel TWM demodulator for both dynamic and static strain measurement.

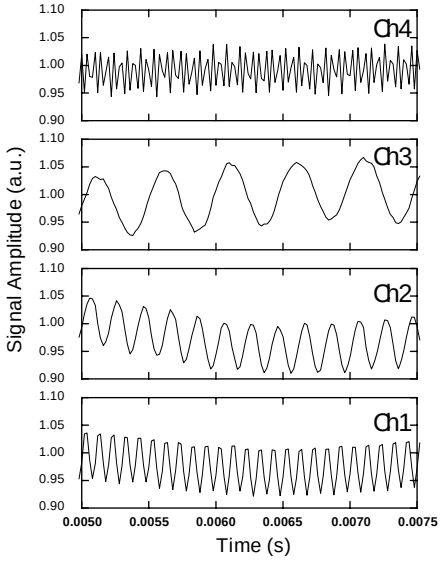

Figure 6 Simultaneous demodulation of the signals from four-FBG sensors using a 4-channel TWM wavelength demodulator.

2.3 Source Location:

The signals from multiple FBG sensors can be used to locate the source of an acoustic event. The FBG sensor is surface mounted on a large aluminum plate of 1mm thickness as shown in Fig. 7. The acoustic emission event is simulated by dropping a 7.9mm steel ball at location 1, 2 and 3 from a controlled height of 1 meter. The FBG sensor is located at position (25cm, 21cm) with respect to the lower left corner of the plate. Figure 8 shows the detected acoustic emission signals at location 1, 2 and 3. From the results, we can clearly see a dispersive plate wave is detected by the FBG sensor.

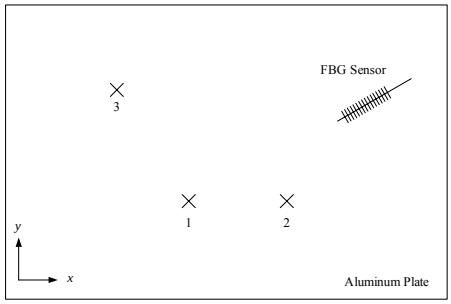

Figure 7: Experimental setup for acoustic emission event detection and source location determination.

The captured time traces then are analyzed using wavelets to determine the location of the ball impact. A Gabor wavelet (mother wavelet) is used to perform the analysis. The experimentally generated dispersion curves are backtracked to identify the location of the impact as follows. The arrival time at each frequency corresponds to the group velocity of the propagating wave. Also the wavelet coefficients obtained at each frequency is strongly dependent on the size of the window and influences the calculated location of the source. To obtain an accurate result, averaging of the localization results obtained with various window sizes is performed to identify the impact location.

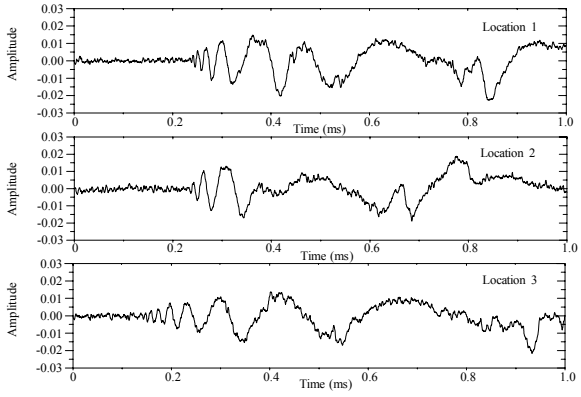

Figure 8 FBG sensor signals detected for the three impact locations

One sensor is used in this analysis to show that the proposed algorithm is suitable for impact location. This enables identification of the source to within a circle. Precise location information through the process of triangulation can be achieved by adding more FBG sensors and applying the same algorithms on the time trace obtained from each sensor.

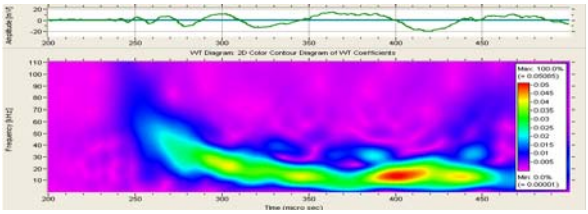

Figure 9. Impact location 1 (a) Response of sensor (b) wavelet transformation of the experimentally generated signal.

Figures 9 shows the time-frequency analysis[13] for one of the impact signals. The experimentally generated dispersion curves can be seen in the wavelet transformation showing the fundamental lower order asymmetric mode of the plate wave. For source location identification, a search algorithm is implemented that identifies the minimum of the difference between locations at two different frequencies for an assumed time. In other words, to start with, the algorithm assumes a vector of time ranging from 0 to 100 microseconds with a small step size. A vector ($Location_{80KHz}$) consisting of the location information at 80 KHz using the group velocity (Cg_{80KHz}) and the assumed time vector ($Time$) is generated using:

$$Location_{80KHz} = Cg_{80KHz} * Time \qquad (2)$$

Similarly, the location information is found for 70KHz using:

$$Location_{70KHz} = Cg_{70KHz} * (Time + \Delta t_{70KHz}) \qquad (3)$$

where $\Delta t_{70KHz} = Time_{80KHz} - Time_{70KHz}$. $Time_{80KHz}$ and $Time_{70KHz}$ are the arrival times determined from Figure 9.

The minimum of the difference between Eqns (2) and (3) indicates the time at which the impact was initiated. The same procedure is repeated for multiple frequencies. Thus at each frequency a value for the likely impact source location is obtained. The predicted locations are shown in Figure 10. A single sensor can predict the location of the impact within the diameter of the circle. Multiple sensors need to be used for more accurate source localization. It is seen that this algorithm provides the impact location quite accurately.

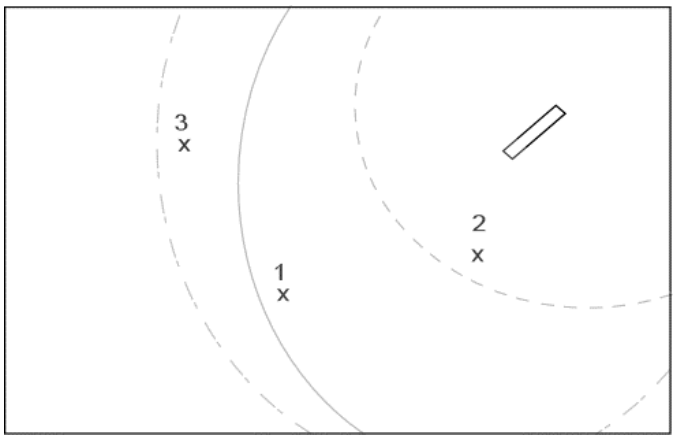

Figure 10. Actual impact location (x) and the predicted impact location (circles).

3. LOW-POWER TWM SPECTRAL DEMODULATOR:

We next present preliminary experimental results on the detection of impact signals using a *low power* (1 mW) TWM demodulation system. Low power operation, while offering significant cost-reduction of the demodulator system, is typically undesirable in TWM interferometers because the intensity of the interacting optical beams in the PRC may not be high enough to achieve fast photorefractive grating formation[12]. This can limit the ability of the interferometer to selectively monitor dynamic wavelength shifts in the presence of low frequency temperature drifts. To overcome this, the interacting beams are focused into the PRC in order to facilitate fast photorefractive grating formation. Furthermore, the TWM gain is optimized through resonant

enhancement of the space charge electric field formed in the PRC by the photorefractive effect using temperature-intensity resonance[14,15].

3.1 Enhancing the TWM Gain using temperature-intensity resonance:

First, the formation of the photorefractive grating in the PRC and beam diffraction was established. An intermittent DC electric field of amplitude 6 KV/cm was applied to the PRC for 10 ms at a repetition rate of 10 Hz. The output of the PRC was measured with the photodetector. The TWM intensity gain (Λ) is defined by the following;

$$\Lambda = \frac{1}{l} In\left(\frac{A_1}{A_2}\right) \qquad (1)$$

where A_1 is the intensity of the transmitted signal beam and the diffracted pump beam, A_2 is the intensity of the transmitted signal beam, l is the length of the PRC, and In is the natural logarithm function. It is seen that Λ is greater than zero when the DC field is applied to the PRC and negligible otherwise. The application of the DC field enhances the space charge electric field and the photorefractive grating formed in the PRC. The TWM gain was measured to be approximately 0.12 cm^{-1} , about four times smaller than the value obtained with the high-power TWM system using the 500 mW source as described earlier. Furthermore, the rise time of the gain plot is less than 2 ms, which gives an estimate of the response time of the PRC. Based on the estimated PRC response time, the expected cut-off frequency of the TWM wavelength demodulation system is close to 500 Hz, which is sufficient to selectively monitor dynamic FBG wavelength shift in the presence of low frequency temperature drifts.

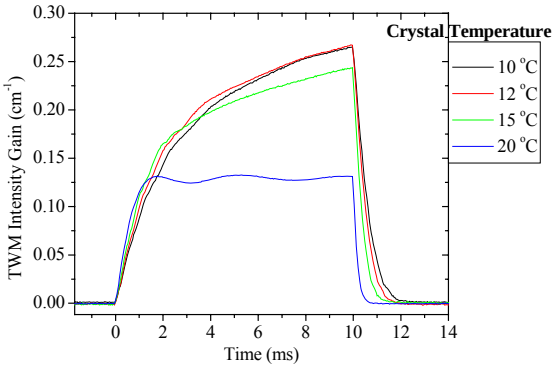

Figure 11. Transient plot of two-wave mixing intensity gain at various values of the PRC temperature

In order to further optimize Λ for efficient wavelength demodulation, the temperature of the PRC was tuned leading to a resonant enhancement of the space charge electric field, a phenomenon referred to as the intensity-temperature resonance[14,15]. The intensity-temperature resonance occurs in InP PRCs operated in the drift mode. In these PRCs, the photorefractive effect involves the thermal- and photo- excitation of both electrons and holes. Typically, thermal excitation of electrons and photo-excitation of holes is dominant in InP, and a resonance condition is obtained when these dominating effects are exactly balanced. As such, for a fixed optical intensity delivered to the PRC, the average temperature in the PRC can be controlled to resonantly enhance the TWM gain. Figure 11 shows the measured TWM gain plots obtained at a few PRC temperatures. The temperature of the PRC is controlled with the thermoelectric cooler. It is seen that the TWM gain increases steadily as the PRC is cooled indicating that resonance occurs at a low temperature for the 1 mW source. The thermoelectric cooler was not stable below 10 ^{o}C, as such, the actual resonance temperature was not ascertained in these experiments. It is noteworthy that the response time of the PRC increases as the resonant temperature is approached, which is due to large charge accumulation in the PRC. Therefore, a trade-off has to be made between TWM gain and PRC response time in choosing the operational temperature.

Preliminary experiments on the demodulation of dynamic strains in a FBG sensor were carried out using the low power system. The strains were produced by impact loading from a ball drop on the aluminum plate. For this experiment, the ball drop location was 14 cm away from the FBG sensor position. The temperature of the PRC was maintained at 12 ^{o}C. The response of the

FBG sensor was compared to the response of a PZT piezoelectric sensor mounted close to the FBG sensor on the plate. A first order low pass filter at 150 KHz was applied to the FBG response to reduce the broadband noise in the signal. The same filter was applied to the PZT response. The FBG and PZT sensor responses are shown in Fig. 12.

Note that the data were taken in single shot mode on the oscilloscope, which was pre-triggered with the PZT response. The transient responses are in good qualitative agreement. The signal to noise ratio (SNR) of the FBG response is low, which is expected because the SNR of the TWM interferometer is proportional to the square root of the optical power in the shot noise limited case. Consequently, the lower the optical power, the lower the SNR. Nevertheless, these experimental results are encouraging in that they indicate that a low power TWM demodulation system can be feasibly implemented, thus allowing for a substantial reduction in the system cost. We are currently exploring the use of high DC fields to improve the SNR of the system.

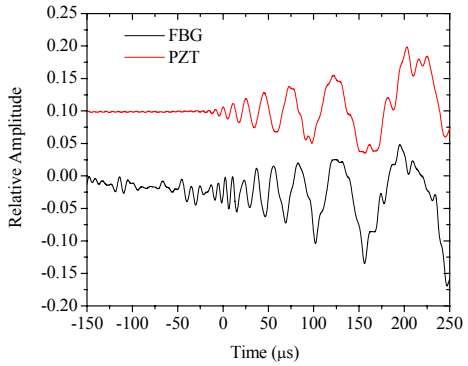

Figure 12. Transient response of FBG and PZT sensors to impact loads on an aluminum plate

CONCLUSIONS

A TWM spectral demodulator is described that can be used for dynamic demodulation of FBG sensors. Multiple FBG's are used to identify the actual location of the impact based on wavelet analysis. Ultrasonic frequencies exceeding 200 KHz were detected by the adaptive FBG demodulator system. The location of the impact was determined with good accuracy. A low-power TWM demodulator is currently being developed to bring the system cost down.

REFERENCES

1. C.S. Sun, and F. Ansari, "Design of the fiber optic distributed acoustic sensor based on Michelson interferometer and its location application," Optical Engineering **42**, 2987-2993 (2003).
2. J. Kiddy, C. Baldwin, T. Salter, T. Chen, "Structural load monitoring of RV Triton using Fiber Optic Sensors," in *Smart Structures and Materials: Industrial and Commercial Applications of Smart Structures Technologies*, Anna-Maria and R. McGowan, eds., Proc. SPIE 4698,462-472 (2002).
3. R. O. Claus, *Fiber Optic Sensor Based Smart Materials and Structures* (Institute of Physics Publishing, PA 1992).
4. F. Ansari., *Fiber Optic Sensors for Construction Materials and Bridges* (Technomic Publishing Co., Lancaster, PA, 1998).
5. B. Culshaw, J. Dakin, *Optical Fiber Sensors: Applications, Analysis, and Future Trends* (Artech House Books, Boston, 1996).
6. E. Udd, *Fiber Optic Smart Structures* (John Wiley, New York, 1995)
7. Grattan and B.T. Meggitt, *Optical Fiber Sensing Technology* (Chapman, UK, 1995).
8. E.Udd, *Fiber Optic Sensors: An Introduction for Engineers and Scientists* (Wiley, New York, 1991).

9. Y.Qiao, “Adaptive demodulation of dynamic signals from fiber Bragg grating sensors using two-wave mixing interferometry in indium phosphide: iron”, *PhD dissertation*, Northwestern University, 2006.
10. Y.Zhou, G.R.Kirikera, S.Krishnaswamy, “Adaptive Fiber Bragg Grating Demodulator for Structural Health Monitoring Applications”, *SAMPE 2007*, Baltimore.
11. Y. Qiao, Y. Zhou, and S. Krishnaswamy, “Adaptive demodulation of dynamic signals from fiber Bragg gratings using two-wave mixing technology”, Appl. Opt. **45**(21), 5132-5142 (2006)
12. L. Solymar, D.J. Webb, and A. Grunnet-Jepsen, “The Physics And Applications Of Photorefractive Materials”, *Oxford University Press Inc.*, New York, 1996
13. M.Takemoto, H.Nishino, K.Ono, “Wavelet Transform – Applications to AE signal analysis” *Acoustic Emission – Beyond the MILLENNIUM*, Edited by T.Kishi, M.Ohtsu, S.Yuyama, Elsevier, 2000, pg 35 – 56.
14. Picoli G., Gravey P., Ozkul C., and Vieux V., “Theory of two-wave mixing gain enhancement in photorefractive InP:Fe : A new mechanism of resonance”, J. Appl. Phys. **66**(8), 3798-3813, (1989)
15. Khelfaoui N., Wolfersgerger D., Kugel G., Fressengeas N., and Chauvet M., “Temporal behavior of two wave mixing in photorefractive InP:Fe versus temperature”, Opt. Comm. **261**, 169-174, (2006)